Journal of the Korean Astronomical Society
49: 73 ∼ 81, 2016 June

http://dx.doi.org/10.5303/JKAS.2016.49.3.73
pISSN: 1225-4614 · eISSN: 2288-890X
http://jkas.kas.org

A Super-Jupiter Microlens Planet Characterized by High-Cadence KMTNet Microlensing Survey Observations of OGLE-2015-BLG-0954

I.-G. Shin[1], Y.-H. Ryu[2], A. Udalski[3], M. Albrow[4], S.-M. Cha[2,5], J.-Y. Choi[6], S.-J. Chung[2], C. Han[7], K.-H. Hwang[7], Y. K. Jung[1], D.-J. Kim[2], S.-L. Kim[2,8], C.-U. Lee[2,8], Y. Lee[2,5], B.-G. Park[2,8], H. Park[6], R. W. Pogge[9], J. C. Yee[1,10], P. Pietrukowicz[3], P. Mróz[3], S. Kozłowski[3], R. Poleski[3,9], J. Skowron[3], I. Soszyński[3], M. K. Szymański[3], K. Ulaczyk[3], Ł. Wyrzykowski[3], M. Pawlak[3], and A. Gould[2,9,11]

[1]Harvard-Smithsonian Center for Astrophysics, 60 Garden St., Cambridge, MA 02138, USA
in-gu.shin,yeonkil.jung,jyee@cfa.harvard.edu
[2]Korea Astronomy and Space Science Institute, 776 Daedeokdae-ro, Yuseong-gu, Daejeon 34055, Korea
yoonhyunryu@gmail.com,chasm,sjchung,keaton03,slkim,leecu,yslee,bgpark@kasi.re.kr,
[3]Warsaw University Observatory, A1. Ujazdowski 4, 00-478 Warszawa, Poland; udalski@astrouw.edu.pl
[4]Department of Physics and Astronomy, University of Canterbury, Private Bag 4800 Christchurch, New Zealand
michael.albrow@canterbury.ac.nz
[5]School of Space Research, Kyung Hee University, Giheung-gu, Yongin, Gyeonggi-do 17104, Korea
[6]Busan National Science Museum, Busan 46081, Korea; quff176@gmail.com,crusader713@hanmail.net
[7]Department of Physics, Chungbuk National University, Seowon-Gu, Cheongju 28644, Korea
cheongho@astroph.chungbuk.ac.kr,kyuha1@gmail.com
[8]Korea University of Science and Technology, 217 Gajeong-ro, Yuseong-gu, Daejeon 34113, Korea
[9]Department of Astronomy Ohio State University, 140 W. 18th Ave., Columbus, OH 43210, USA
pogge@astronomy.ohio-state.edu
[10]Sagan Fellow
[11]Max-Planck-Institute for Astronomy, Königstuhl 17, 69117 Heidelberg, Germany; gould@astronomy.ohio-state.edu

Received February 27, 2016; accepted April 27, 2016

Abstract: We report the characterization of a massive ($m_p = 3.9 \pm 1.4 M_{\rm jup}$) microlensing planet (OGLE-2015-BLG-0954Lb) orbiting an M dwarf host ($M = 0.33 \pm 0.12 M_\odot$) at a distance toward the Galactic bulge of $0.6^{+0.4}_{-0.2}$ kpc, which is extremely nearby by microlensing standards. The planet-host projected separation is $a_\perp \sim 1.2$ AU. The characterization was made possible by the wide-field ($4\,{\rm deg}^2$) high cadence ($\Gamma = 6\,{\rm hr}^{-1}$) monitoring of the Korea Microlensing Telescope Network (KMTNet), which had two of its three telescopes in commissioning operations at the time of the planetary anomaly. The source crossing time $t_* = 16$ min is among the shortest ever published. The high-cadence, wide-field observations that are the hallmark of KMTNet are the only way to routinely capture such short crossings. High-cadence resolution of short caustic crossings will preferentially lead to mass and distance measurements for the lens. This is because the short crossing time typically implies a nearby lens, which enables the measurement of additional effects (bright lens and/or microlens parallax). When combined with the measured crossing time, these effects can yield planet/host masses and distance.

Key words: gravitational microlensing — planets

1. Introduction

The Korea Microlensing Telescope Network (KMTNet; Kim et al. 2016) is a system of three 1.6m telescopes, each equipped with a $4\,{\rm deg}^2$ 340-Mpixel camera, located in Chile, South Africa, and Australia. The system was designed to conduct a microlensing survey that would detect Earth-mass planets without additional followup data. While microlensing events typically last for tens of days, many of their most interesting features occur on much shorter timescales, especially features that permit the detection and characterization of planets, which have typical perturbation times

$$t_p \sim \sqrt{\frac{m_p}{M_{\rm jup}}}\,{\rm day} \sim 1.3\sqrt{\frac{m_p}{M_\oplus}}\,{\rm hr}, \qquad (1)$$

where m_p is the mass of the planet.

Most microlensing planets have been discovered by combining survey and followup observations. In their original suggestion of this approach, Gould & Loeb (1992) argued that Galactic bulge fields should be monitored at relatively low cadence (e.g., once per night). This would enable them to cover the widest possible area, which is necessary to detect a large sample of microlensing events in spite of their low frequency $\Gamma \sim 10^{-5}{\rm yr}^{-1}\,{\rm star}^{-1}$, but would not generally per-

Corresponding author: A. Gould

mit the detection of planets. Hence, the survey teams would have to alert the community to these events in real time, allowing followup networks to initiate high-cadence monitoring of individual events.

The effectiveness of this survey+followup approach was greatly increased by the recognition that the sensitivity of microlensing events to planets is dramatically increased at high magnification (Griest & Safizadeh 1998). This permitted scarce observing resources to be focused on the rare subset of high-mag events, with the observations concentrated on the brief interval near peak. A spectacular example of the success of this approach was the discovery of the Sun/Jupiter/Saturn analog OGLE-2006-BLG-109L (Gaudi et al. 2008; Bennett et al. 2010). Despite its successes, this approach of combining survey and followup observations is highly inefficient and allows only a small subset of events to be observed with a high enough cadence to detect planets. See Gould et al. (2010) for a thorough review of this approach.

Even from the beginning, however, an alternate approach of survey-only detections yielded a significant fraction of all planet detections. For example, the very first microlensing planet OGLE-2003-BLG-235Lb was discovered in this mode (although the planet characterization benefited substantially by "auto-followup" by the MOA group) (Bond et al. 2004). This event was unusual in that the planetary perturbation lasted several days, which is what enabled characterization given the surveys of that time. However, these survey characteristics also permitted the survey-only detection of a variety of other planetary events, including the fleeting planetary signal in the high-magnification event MOA-2007-BLG-192 (Bennett et al. 2008). Moreover, survey-only coverage yielded key light-curve features even in some events for which the main features were discovered in survey+followup mode, such as OGLE-2006-BLG-109L, mentioned above.

Nevertheless, as soon as the first microlensing planet was discovered, it was clear that by augmenting the camera size, one could cover the same area at much higher-cadence observations that would be capable of detecting and characterizing planets without followup. This insight ultimately led to the MOA-II and OGLE-IV experiments, which were commissioned in 2006 and 2010, respectively.

In 2004, Cheongho Han initiated discussions with colleagues that led to the design of a more far-reaching variant of this approach: construct very wide-field cameras on the three southern continents. By virtue of their large fields of view, these telescopes could both monitor very wide areas and do so at a rapid cadence (i.e., several times per hour). Their geographic distribution would allow nearly continuous coverage of events. Thus, such a survey would not only detect microlensing events but would also be able to characterize planetary perturbations. Hence, this approach allows all events to be monitored for planets and eliminates the need for real-time followup observations. A smaller scale variant of this approach was achieved by combining the OGLE, MOA and Wise surveys (Shvartzvald & Maoz 2012; Shvartzvald et al. 2016).

A natural consequence of this approach is that all features in the microlensing light curve are automatically monitored at high cadence. Aside from just detecting the planetary perturbations, it is important to capture the caustic crossings because, if they are resolved, they provide crucial additional information about the lens. Caustic crossings occur in the great majority of published planetary and binary events. While there is some publication bias hidden in this statistic, detailed simulations show that even with systematics-free data, at least half of all recognizable planetary events have caustic crossings (Zhu et al. 2014, 2016).

The duration of the crossing allows one to determine the normalized source size

$$\rho = \frac{\theta_*}{\theta_{\rm E}}\,;\ \theta_{\rm E} \equiv \sqrt{\kappa M \pi_{\rm rel}}\,;\ \kappa \equiv \frac{4G}{c^2 {\rm AU}} \simeq 8.14\,\frac{\rm mas}{M_\odot} \quad (2)$$

where θ_* is the angular radius of the source, $\theta_{\rm E}$ is the Einstein radius, M is the lens mass, and $\pi_{\rm rel} = {\rm AU}(D_L^{-1} - D_S^{-1})$ is the lens-source relative parallax. Since θ_* is almost always measurable by standard techniques (Yoo et al. 2004), this yields a measurement of $\theta_{\rm E}$ and thus of the product $M\pi_{\rm rel}$, which can be a crucial constraint in the interpretation of the lens.

Typical source sizes are $\theta_* = 0.6\,\mu{\rm as}$, and typical lens-source relative proper motions are $\mu_{\rm rel} = 4\,{\rm mas\,yr^{-1}}$. Hence, caustic crossing times are similar in duration to Earth-mass planetary perturbations

$$t_{\rm cc} = t_* \sec\phi\,,\ t_* \equiv \frac{\theta_*}{\mu_{\rm rel}} = 1.3\,{\rm hr}\,\frac{\theta_*}{0.6\,\mu{\rm as}}\left(\frac{\mu}{4\,{\rm mas/yr}}\right)^{-1}, \quad (3)$$

where t_* is the source self-crossing time, $t_{\rm cc}$ is the caustic crossing time and ϕ is the angle of crossing. Therefore, resolving a caustic crossing requires the same cadence as detecting Earth-mass planets.

Although considerable effort is exerted by followup groups to monitor caustic crossings of "interesting" events, in practice this is difficult and suffers from many of the same problems as followup searches for planets. At least half of all caustic crossings (i.e., caustic entrances) are essentially impossible to predict from the pre-crossing light curve, and a fair fraction of the rest (i.e., caustic exits) are quite difficult to predict. In addition, many caustic exits occur when they are unobservable from a given location on Earth due to sidereal time or weather. Moreover, many events that turn out to be "interesting" are not recognized as such until after the time of the crossing. This makes high-cadence, round-the-clock surveys such as KMTNet a game-changer for planetary and binary science.

Here we present a planetary microlensing event, OGLE-2015-BLG-0954, that showcases KMTNet's ability to resolve unexpected caustic crossings of exceptionally short duration. We show that capturing the crossing was crucial to the interpretation of this planetary system.

2. KMTNet

The three KMTNet telescopes were all commissioned in the 2015 bulge season, taking their first scientific data in February (South Africa), March (Chile), and June (Australia). During this commissioning season, they simultaneously took scientific data and underwent various engineering tests and adjustments. While the system was only fully operational at the end of the season, the data quality are generally quite high. For example, these data played an important role in the characterization of the massive-remnant binary candidate OGLE-2015-BLG-1285La,b (Shvartzvald et al. 2015).

The system is designed to monitor a large field at a rapid cadence (Kim et al. 2016). The pixel scale was optimized for microlensing at $0.4''$ to cover the widest possible area while still being Nyquist sampled at typical good seeing at the best site (Chile). The cadence was selected based on Equation (1) which shows that it should be of order 4–6 hr^{-1} to enable approximately a dozen measurements over the perturbation time of an Earth-mass planet $2t_{p,\oplus} \sim 3\,\mathrm{hr}$. Indeed simulations by Henderson et al. (2014) show that as one increases the observing area (and correspondingly decreases the cadence) with a KMTNet-like system, the number of planet detections of all types increases at first. However, at cadences of about $5\,\mathrm{hr}^{-1}$, the number of Earth detections reaches a maximum while the detections of more massive planets continues to rise. Hence, the survey strategy adopted in 2015 was to observe 4 fields (so $16\,\mathrm{deg}^2$) at about $6\,\mathrm{hr}^{-1}$. In addition, other fields were also observed at much lower cadence in pursuit of other science objectives.

3. OGLE-2015-BLG-0954's Unforeseen Caustic Crossing

On 10 May 2015, the Optical Gravitational Lens Experiment (OGLE) Early Warning System (EWS, Udalski et al. 1994; Udalski 2003) alerted the microlensing community to a new event, OGLE-2015-BLG-0954 at (α, δ)=(18:00:44.24,−28:39:39.2), $(l, b) = (1.9, -2.7)$. At $\mathrm{HJD}' = 7164.62$ (UT 02:45 22 May) the event began a caustic entrance, which led to a jump of about 1 magnitude between the first and second OGLE points of the night, which were separated by 105 minutes. These were posted to the EWS website when OGLE next updated it, shortly after UT 15:01 22 May, i.e. $\mathrm{HJD}' = 7165.12$, which happened to be almost exactly the time of the end of the caustic exit $\mathrm{HJD}' = 7165.15$. Hence, there was essentially no time to organize observations of the caustic exit. In any case, there were no such attempts of which we are aware.

4. Observations

OGLE-2015-BLG-0954 was observed only by the OGLE and KMTNet collaborations. There were no followup observations.

OGLE observations were carried out with the 1.3m Warsaw Telescope at Las Campanas, Chile. The event lies in OGLE field BLG512, which means that is normally observed at 20 minute cadence in I band, with occasional V-band observations to determine the source color. The 105-minute gap reported above is therefore unusual. There are no observing-log notes on this hiatus, but given the conditions at neighboring CTIO (see below), we suspect that the observer considered the conditions at LCO as unacceptable.

KMTNet scientific observations commenced on 10 March, 21 February, and 20 June in Chile (CTIO), South Africa (SAAO), and Australia (SSO), respectively. Overall the data from CTIO, SAAO, and SSO are of good science quality, but the commissioning observations were impacted by a variety of engineering-related issues ranging from breaks in the schedule to adjustment of the detector electronics. In the case of the CTIO data there are two times when the detector electronics changed substantially. We therefore fit the CTIO light curves as three independent curves (to avoid introducing artifacts into long term effects, particularly parallax), with breaks at $\mathrm{HJD}' = 7130$ and $\mathrm{HJD}' = 7192$. We also note that because the SSO observations began well after the caustic crossing, they do not contribute substantially to the analysis, but are included for completeness.

The majority of data taken at CTIO and all the data taken at SAAO and SSO were taken in I-band, with respectively 2132, 1350, and 449 points included in this study. V-band observations were made in Chile only, for the purpose of determining the source color. See Section 6. The ratio of V:I observations in Chile is about 1:5. Only the second segment of Chile data were used for this purpose because this is the only segment that has sufficient flux variation to accurately constrain the source color. There are 113 V-band points that could be matched to a corresponding I-band point within 1.2 hours and so are used in this color determination.

Observations during the caustic crossing were taken in quite unstable weather conditions. The crossing lasted $2t_{\mathrm{cc}} = 33\,\mathrm{min}$. Of the three points taken during this crossing, one image could not be reduced and the remaining two have formal errors that are respectively 3 and 2 times larger than typical errors at the same brightness during the rest of the night. Conditions recovered immediately after the caustic entrance. KMTNet policy is to take observations regardless of seeing and with up to 6 magnitudes of extinction by clouds. The great majority of observations taken in poor conditions are "useless" in the sense that the information content of neighboring points far exceeds that of these poor-condition data. However, as Lao Tzu[1] foretold, these "useless" data can prove crucial.

The modeling was conducted based on reductions using image subtraction (Albrow et al. 2009; Alard & Lupton 1998). DoPhot (Schechter et al. 1993) reductions were used to determine the source color and magnitude.

[1] "Any man can make use of the useful, but it takes a wise man to make use of the useless."

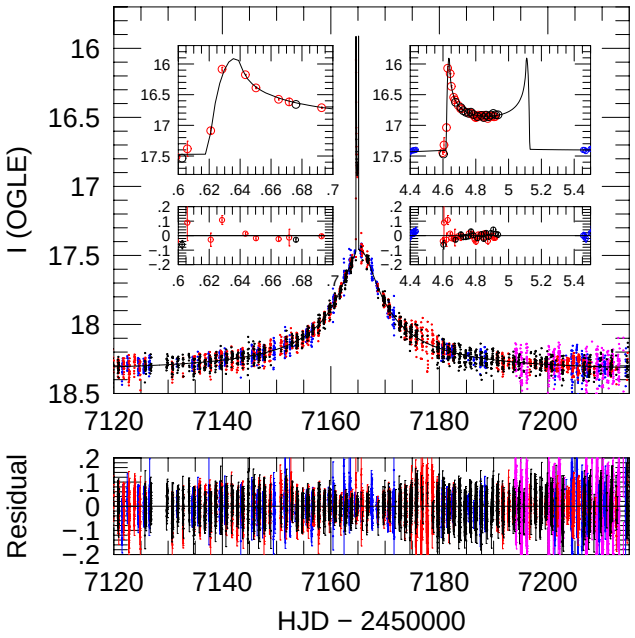

Figure 1. Light curve and best-fit model for OGLE (black) and KMTNet observations of OGLE-2015-BLG-0954 with KMTNet data from Chile (red), South Africa (blue) and Australia (magenta). Insets show the caustic, which extends from 7164.62 to 7165.15. Error bars are omitted from the main figure to avoid clutter but are shown in the residuals.

5. LIGHT CURVE MODEL

Figure 1 shows the light-curve data from OGLE and the three KMTNet observatories together with the best fitting model. With the exception of a brief half-day eruption at peak, the light curve looks qualitatively like a standard point lens event that might adequately be parameterized by just three parameters, $(t_0, u_0, t_{\rm E})$, i.e., the time of lens-source closest approach, the impact parameter (normalized to $\theta_{\rm E}$), and the Einstein crossing time. The caustics at peak imply that this is a binary or planetary lens, which then requires three more parameters (s, q, α), the separation of the two masses (normalized to $\theta_{\rm E}$), their mass ratio, and their orientation relative to the lens-source proper motion $\boldsymbol{\mu}_{\rm rel}$. The fact that the caustic entrance is resolved means that the normalized source radius ρ is also required for the model. In addition, source and blend fluxes (f_s, f_b) must be fit for each independent data set (3 from CTIO and 1 from each of the others). We conduct a broad search over (s, q) geometries, allowing the other five parameters to vary continuously from seed solutions that are well sampled in α. We find only two local minima, which are related by the well known close/wide binary degeneracy (Griest & Safizadeh 1998; Dominik 1999). The parameters for these two solutions are given in Table 1.

There are two major striking features of these solutions. First, the planet/star mass ratio is 0.011 (or 0.012), i.e., about 11 or 12 times that of Jupiter/Sun.

Table 1
Microlensing parameters for OGLE-2015-BLG-0954

Parameter	Unit	Close	Wide
χ^2 /dof		12909.1 / 12916	12908.6 / 12916
$t_0 - 7100$	day	65.223 0.009	65.220 0.009
u_0		−0.0568 0.0017	−0.0580 0.0021
$t_{\rm E}$	day	37.53 0.87	36.96 1.10
s		0.7982 0.0033	1.3522 0.0063
q		0.01098 0.00028	0.01194 0.00043
α	radian	4.5462 0.0044	4.5890 0.0044
ρ	10^{-4}	2.96 0.11	3.03 0.13

Second, the self-crossing time is extremely quick,

$$t_* = \rho t_{\rm E} = 16.0 \pm 0.5\,{\rm min}. \quad (4)$$

Comparison with Equation (3) shows that either the source must be extremely small or $\mu_{\rm rel}$ must be very high.

6. COLOR-MAGNITUDE DIAGRAM

Figure 2 is a calibrated color-magnitude diagram (CMD) showing field stars within 90″ of the lens from the OGLE-III catalog (Szymański et al. 2011) together with the source position determined from the model presented in Section 5, as well as the blend.

To construct this diagram, we make two, basically independent measurements, using KMTNet and OGLE data, respectively

For the KMTNet measurement, we first measure the source in an instrumental system based on DoPhot photometry using regression for the $(V - I)$ color and a fit to the best model for the I magnitude, respectively. We then put these on the OGLE-III system via a transformation derived from common field stars. We find $((V-I), I)_s = (2.01 \pm 0.05, 20.92 \pm 0.03)$, where the error in the color is due to the scatter in the photometric data, while the error in the magnitude is primarily due to a highly correlated $\sim 3\%$ error in the parameters $(f_s, u_0, t_{\rm E}, q, \rho)$. See Table 1 and Yee et al. (2012).

We repeat this procedure using OGLE-IV light-curve data, which is calibrated in I but not V. We find $((V - I), I)_s = (1.91 \pm 0.07, 20.90 \pm 0.03)$. Noting that the errors in the color are independent but those in the magnitude are not, we combine the two measurements to obtain $((V - I), I)_s = (1.98 \pm 0.04, 20.91 \pm 0.03)$.

To derive the calibrated blend (i.e., non-source) light, we subtract the fluxes corresponding to these

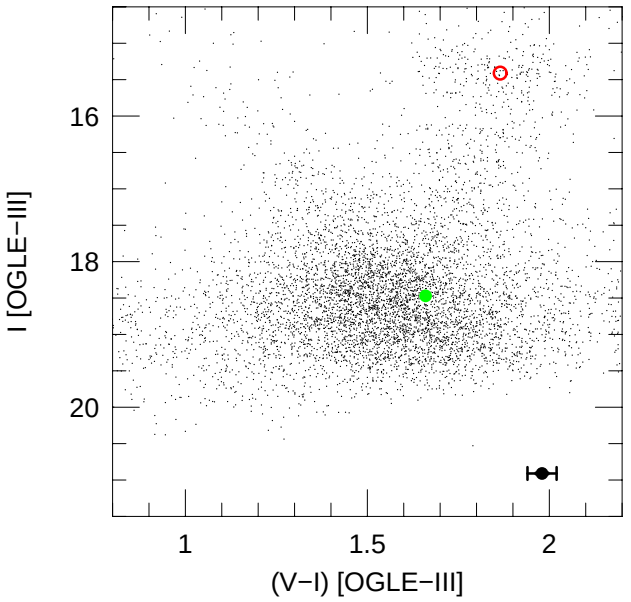

Figure 2. Calibrated color magnitude diagram showing the microlensed source (black) and the blended light (green) relative to the centroid of the red clump (red). The field stars are taken from the OGLE-III catalog (Szymański et al. 2011). The source color and magnitude are derived in instrumental systems, and then transformed to the OGLE-III system using field stars. The blended light is derived by subtracting the source (V, I) fluxes from the (V, I) fluxes of the baseline object found in the OGLE-III catalog.

magnitudes from those of the OGLE-III star at this position, with $((V-I), I)_{\rm base} = (1.69, 18.36)$ to obtain $((V-I), I)_b = (1.66, 18.47)$. The errors in these quantities are essentially the same as those of the baseline flux because the blend fluxes are almost the same as the baseline fluxes. We estimate these as 0.07 and 0.02 magnitudes respectively.

Assuming that the source is behind the same amount of dust as the clump, we can determine its intrinsic color and magnitude and use those values to determine $\theta_{\rm E}$. First, we measure the position of the red clump: $((V-I), I)_{\rm cl} = (1.87, 15.41)$. Given the intrinsic clump position $((V-I), I)_{0,\rm cl} = (1.06, 14.38)$ (Bensby et al. 2013; Nataf et al. 2013), we then derive $((V-I), I)_{0,s} = (1.17, 19.88)$. Then using the VIK color-color relations of Bessell & Brett (1988) and the color-surface brightness relations of Kervella et al. (2004), we derive an angular source radius,

$$\theta_* = 0.56\,\mu{\rm as}. \qquad (5)$$

The resulting angular size of the Einstein ring and lens-source relative proper motion are

$$\theta_{\rm E} = \frac{\theta_*}{\rho} = 1.89\,{\rm mas}\,; \quad \mu_{\rm rel} = \frac{\theta_{\rm E}}{t_{\rm E}} = 18.4\frac{\rm mas}{\rm yr}\,. \qquad (6)$$

All three quantities have the same 9% error, which we calculate as follows. The 3% modeling flux error contributes half (Yee et al. 2009), i.e., 1.5%. Centroiding the clump in I contributes 4%. There is a 0.04 mag measurement error in the color and another 0.06 mag error in deriving the surface temperature from the microlensing color (Bensby et al. 2013), which together propagate to a 6% error. Finally, there is a 5% error from propagating the scatter in the VIK relations.

7. The Nature of the Lens

7.1. A Nearby Lens

The measured $\theta_{\rm E}$, blended light, and proper motion strongly imply a nearby lens.

7.1.1. $\theta_{\rm E}$ and the CMD

We can conclude with near certainty that lens is in the near disk from the large Einstein radius combined with limits on the light from the lens, which cannot be brighter than the observed blended light. The $\theta_{\rm E}$ measurement provides a constraint from $\theta_{\rm E}^2 = \kappa M \pi_{\rm rel}$, i.e.,

$$M = (1.0 \pm 0.18) M_\odot \left(\frac{\pi_{\rm rel}}{0.44\,{\rm mas}}\right)^{-1}. \qquad (7)$$

Suppose that the lens were a $M = 1\,M_\odot$ star, and therefore at 1.75 kpc. Even if it were behind the same amount of dust as the clump ($A_I = 1.05$, Nataf et al. 2013) and were somewhat subluminous at $M_I = 4.5$, it would be $I \sim 16.75$, about 1.7 mag brighter than the observed blend. In addition, it would be somewhat bluer. Essentially the same argument applies to any host $M \gtrsim 0.25\,M_\odot$ (i.e, $\pi_{\rm rel} = 1.76\,{\rm mas}$, $M_I \sim 9$ $\Rightarrow$ $I = 18.67$). That is, it results in a solution that contradicts the observed blend.

Note that at the limit $M = 0.25 M_\odot$, the photometric constraint from the blended light would still not be truly satisfied. That is, although the lens would contribute less than the observed I-band light, the color would still be wrong. Such a star would contribute only about 15% of the observed V-band light, meaning the other 85% would then have to be supplied by another star. Of course, there could be such an object, but it would itself contribute substantial I-band light. When combined with the lens light, the total light would then exceed the limit unless the lens were yet fainter than we have just supposed.

On the other hand, if $\theta_{\rm E}$ were 2σ smaller, this would allow for smaller $\pi_{\rm rel}$ at fixed mass, and hence, a more distant lens. This consequent 0.4 mag reduction in flux from the lens would provide the necessary margin to accommodate light from an additional star.

Taking all of these considerations into account, we therefore regard $M < 0.25 M_\odot$ as a conservative photometric upper limit on the host mass. This gives a corresponding upper limit on the lens distance of 0.5 kpc. This leads to the conclusion that the lens is a very-low mass, nearby object and may even be a brown dwarf.

The only exception to this line of reasoning would be stellar remnants, either white dwarfs, neutron stars, or black holes. These are generally believed to have few

planets so we do not further pursue this possibility here. As we discuss in Section 8.3, if future observations show that the lens is not contributing to the blend light then this question should be revisited.

7.1.2. Lens-Source Relative Proper Motion

The lens-source relative proper motion, $\mu_{\rm rel} = 18\,{\rm mas\,yr^{-1}}$ (Equation 6), also suggests a nearby lens. This value is much higher than for typical bulge lenses ($\sim 4\,{\rm mas\,yr^{-1}}$) or far-disk lenses ($\sim 7\,{\rm mas\,yr^{-1}}$), which are dominated by internal stellar motions in the bulge and the flat rotation curve of the Galaxy, respectively. However, the proper motions of very nearby lenses are dominated by their peculiar motion, $v_{\rm pec} \sim \mathcal{O}(50\,{\rm km\,s^{-1}})$, i.e., $\mu_{\rm rel} \to v_{\rm pec}/D_L$. This can be arbitrarily large for sufficiently nearby lenses. For example, the extremely nearby lens OGLE-2007-BLG-224 ($D_L = 0.5\,{\rm kpc}$) had a record proper motion of $\mu_{\rm rel} = 48\,{\rm mas\,yr^{-1}}$ (Gould et al. 2009). While the observed proper motion does not definitively rule out either the bulge-lens or far-disk lens scenarios, it is most easily explained by a nearby lens.

7.2. Lens Properties

Given our conclusion that the lens is nearby, we can estimate its mass and distance based on the velocity distribution of stars in the nearby disk. The projected transverse velocity $\tilde{v} \equiv {\rm AU}\mu_{\rm rel}/\pi_{\rm rel}$ is typically 50 km s^{-1}, and the lens mass is related to $\tilde{v}$ by

$$M = \frac{c^2}{4G}\tilde{v}t_{\rm E}\theta_{\rm E} \to 0.25\,M_\odot \frac{\tilde{v}}{50\,{\rm km\,s^{-1}}}, \qquad (8)$$

where we have substituted in the best fit values for $\theta_{\rm E}$ and $t_{\rm E}$ in the last step. Similarly,

$$\pi_{\rm rel} = \frac{{\rm AU}\mu_{\rm rel}}{\tilde{v}} \to 1.7\,{\rm mas}\left(\frac{\tilde{v}}{50\,{\rm km\,s^{-1}}}\right)^{-1} \qquad (9)$$

Since, the rms projected velocity of nearby stars is $\tilde{v} \sim 50\,{\rm km\,s^{-1}}$, these are plausible first estimates for the lens mass and relative parallax. They are roughly consistent with the upper limits derived in Section 7.1.1.

However, we can also make a purely kinematic estimate ignoring the flux constraints. This is appropriate either to allow for dark (or very dim hosts) such as white dwarfs, or to allow for larger-than-expected errors in $\theta_{\rm E}$ (which entered these constraints), due to either large statistical fluctuations or to unrecognized systematic errors.

To do so, we must also weight our results to account for the transformation between microlensing parameters and the physical parameters of the system. This accounts for the underlying bias of the observations toward more distant and thus (given that $M\pi_{\rm rel} = \theta_{\rm E}^2/\kappa$ is measured) more massive lenses.

For fixed (i.e., measured) $\theta_{\rm E}$ and $\mu_{\rm rel}$, the probability is weighted by the volume element $(dD_L\, D_L^2)$ as well as the stellar density variation (which in the present case is minor). Approximating the projected velocity distribution[2] as a Gaussian with 1-D dispersion $\sigma = 50\,{\rm km\,s^{-1}}/\sqrt{2}$, one may write,

$$\langle M \rangle = \frac{\int dD_L [D_L(\tilde{v})]^2 M(\tilde{v}) \tilde{v} \exp(-\tilde{v}^2/2\sigma^2)}{\int dD_L [D_L(\tilde{v})]^2 \tilde{v} \exp(-\tilde{v}^2/2\sigma^2)}, \qquad (10)$$

where M and D_L are regarded as implicit functions of $\tilde{v}$ through Equations (8) and (9), respectively. Then using the near-field approximation $D_L \to {\rm AU}/\pi_{\rm rel}$, one may easily derive

$$M = \frac{c^2}{4G}\sqrt{2}\sigma\left(\frac{3\sqrt{\pi}}{4}\right)t_{\rm E}\theta_{\rm E} \to 0.33 \pm 0.12\,M_\odot \qquad (11)$$

and similarly for $\pi_{\rm rel}$,

$$\pi_{\rm rel} = \frac{{\rm AU}\mu_{\rm rel}}{\sqrt{2}\sigma}\left(\frac{\sqrt{\pi}}{2}\right) \to 1.5 \pm 0.6\,{\rm mas}. \qquad (12)$$

These estimates are consistent at the 1-σ level with the host-mass limit $M < 0.25\,M_\odot$ that was derived in Section 7.1.1 and also at the 1.5-σ level with typical white-dwarf masses. In Section 8.3, we discuss how this ambiguity can be resolved. Until that time, we adopt the above kinematic estimates, which straddles both cases. Then, combining Equation (11) with the planet-star mass ratio $q = 0.0115$ (average of the two solutions) yields an estimated planet mass,

$$m_{\rm planet} = 3.9 \pm 1.4\,M_{\rm jup}. \qquad (13)$$

When high-resolution imaging resolves the nature of the host (Section 8.3), this estimate can be made more precise.

Because the distance uncertainty is roughly 30% and the two solutions (wide and close) are roughly equally likely, the estimates of the projected separation from these two solutions overlap. We therefore estimate

$$a_\perp = D_L\theta_{\rm E}s \to 1.2 \pm 0.6\,{\rm AU}. \qquad (14)$$

Note that while some of this large uncertainty can be removed by resolving the host, the dichotomy between close and wide solutions will remain.

8. WHAT IS THE NATURE OF THE BLENDED LIGHT?

8.1. Astrometry

To probe the relation of the blended light to the event, we first determine whether or not it is coincident with the position of the lens by measuring the centroid of the source-blend combined light. We compare the apparent position of the source-blend combined light when the source is highly magnified on HJD$' \sim 7187.7$ (when the source accounts for 65% of the total light) to its position

[2] We estimate $2\sigma^2 = \sigma_\phi^2 + \sigma_z^2 + v_{\oplus,\perp}^2 + [(D_L/D_S)v_{\rm rot}]^2$ where $(\sigma_\phi, \sigma_z) = (33, 18)\,{\rm km\,s^{-1}}$ are the Galactic velocity dispersions of the disk in the rotation and vertical directions, $v_{\oplus,\perp} = 25\,{\rm km\,s^{-1}}$ is Earth's speed relative to the LSR at the peak of the event, and $(D_L/D_S)v_{\rm rot} = {\rm km\,s^{-1}}$ is the projection of Galactic rotation. This would yield $\sqrt{2}\sigma = 48\,{\rm km\,s^{-1}}$, which we round to $50\,{\rm km\,s^{-1}}$.

near baseline (when it accounts for about 13%). We conduct two independent measurements, using KMTNet and OGLE data, respectively, employing somewhat different procedures for the two cases.

For the KMTNet data, we consider 33 CTIO images with seeing FWHM $< 1.35''$, including 7 from the above mentioned highly magnified night and 26 that are at least 25 days from peak (so magnified $A < 1.8$). Because the baseline object is relatively isolated (with only one relevant near-neighbor, which is at $1.4''$), we fit directly to the flux counts of individual pixels in the vicinity of the lens, taking account of this neighbor. We find that the offset between these two groups (peak minus baseline) is -60 ± 25 mas and 0 ± 27 mas in the East and North directions. This implies separations between the source and blend of -120 ± 50 mas and 0 ± 54 mas, respectively.

For the OGLE data we compare the apparent position of the difference image (isolated PSF obtained from magnified image minus template) near maximum to the DoPhot position of the apparent source (really source+blend) at baseline (mean epoch 2010.8). We find offsets of -80 ± 25 mas and $+105 \pm 25$ mas in the East and North directions, which corresponds to separations between the source and blend of -90 ± 30 mas and $+120 \pm 30$ mas, respectively.

Naively, the OGLE and KMTNet measurements are consistent at much better than $1\,\sigma$ in the East direction but disagree at $2\,\sigma$ in the North direction. This itself is hardly unusual and would be expected $\exp(-2^2/2) = 14\%$ of the time. Moreover, we must bear in mind that these two measurements are not necessarily measuring the same thing. After some algebra, one may show that if the blend is associated with the lens (being either the lens itself or a companion to the lens), then one expects the OGLE and KMTNet measurements to differ by $\vec{\mu}\Delta t \sim 85$ mas, where $\mu = 18\,\mathrm{mas\,yr^{-1}}$ in some unknown direction and $\Delta t \sim 4.7$ yr. Hence, the two measurements may be more consistent than first appears.

In brief, both the OGLE and KMTNet measurements give a consistent measurement of the separation between they source and the blend. They are both consistent at the 2-σ level with zero separation between the source and blend. At the same time, if the source and blend are not coincident, these measurements place an upper limit on their separation of 200 mas. Hence, there is no clear evidence that the blended light is displaced from the source. We discuss how to improve this constraint in Section 8.3.

8.2. Four Possible Origins of Blended Light

8.2.1. Blend as Unrelated Star

There are 3500 stars brighter than the blend within $90''$ of the lens. Hence, the chance of one of these being projected within 200 mas is $3500 \times (0.2/90)^2 = 1.7\%$. While this probability is small, such random projection is not implausible.

8.2.2. Blend as Companion to the Source

Another possibility is that the blend is a subgiant companion to the source. Roughly 15% of G dwarfs have companions $M_{\rm comp}/M_G > 0.8$ and with semimajor axes $a \lesssim 200\,\mathrm{mas} \times 8\,\mathrm{kpc} = 1600\,\mathrm{AU}$ (Raghavan et al. 2010). Since reddish subgiants $(V-I)_0 \gtrsim 0.9$ live about 10 times shorter than such upper main-sequence stars, the probability of such a companion is about 1.5%, i.e., similar to the first scenario.

8.2.3. Blend as the Host

The remaining possibility is that the blend is part of the lens system, either the host itself or a companion to it that is too far separated to influence the magnification.

It is difficult to come up with a plausible host that explains the blended light for reasons that are closely related to the fact that the blended light places upper limits on the host light, as discussed in Section 7.1.1. For example, if the blend were behind all the dust, then its color would imply a late G dwarf of mass $M \sim 0.9\,M_\odot$. Identifying this star with the host would then imply, via Equation (7), $D_L = 1.6$ kpc, and so $M_I = 6.4$. This is substantially too dim for typical late G dwarfs. On the other hand, if the lens were in front of all the dust, its color would imply a late K dwarf, $M \sim 0.6\,M_\odot$ and so (assuming it were the host) $\pi_{\rm rel} = \theta_{\rm E}^2/\kappa M = 0.73$ mas, i.e., $D_L \sim 1.2$ kpc and so $M_I = 8.1$. Again, this is substantially too dim for late K dwarfs.

8.2.4. Blend as Companion to the Host

Another possibility is that the blended light is a companion to the host. However, it is also not easy to arrange for this scenario. For example, if the blend is in front of all the dust, then its color implies a late K dwarf, so $M_I \sim 6$. Then its apparent magnitude implies $D_L = 3$ kpc, and so $\pi_{\rm rel} \sim 0.2$ mas. But that implies the host would be $M \sim 2.5\,M_\odot$, which would produce an obvious flux contribution (unless it were a dark remnant).

Hence, although the probabilities for a random interloper (Section 8.2.1) and a companion to the source are modest (Section 8.2.2), these are the most likely scenarios.

8.2.5. Blend as Combination of Two or More Stars

Finally, of course, it is possible that the blended light is due to two or more stars. If both were drawn from the first two possibilities above (source companion or random interloper) then the prior probability would be roughly the square of the probabilities calculated there, i.e., $\sim 3 \times 10^{-4}$. However, it is also possible that star light from one of these two possibilities is combined with light from the lens system (host or companion). The large range of such possible combinations would then imply that high-resolution imaging would be required to extract a unique interpretation. We discuss this in the next section.

8.3. Resolution

Several types of information can be assembled on various timescales to resolve the nature of the host. First, it should be possible to immediately measure the heliocentric proper motion of the baseline-object using OGLE-III data (e.g., Skowron et al. 2013). If the proper motion is high, then it is very likely that the blended light is either the host itself or that it is a companion to the host. Note that in interpreting such a measurement one must account for the difference between heliocentric and geocentric proper motion,

$$\boldsymbol{\mu}_{\rm hel} - \boldsymbol{\mu}_{\rm geo} = \mathbf{v}_{\oplus,\perp}\frac{\pi_{\rm rel}}{\rm AU} = (0.29, 5.41)\frac{\pi_{\rm rel}}{\rm yr} \qquad (15)$$

where we have substituted in the value of $\mathbf{v}_{\oplus,\perp}$, Earth's instantaneous projected velocity at the peak of the event, in (north,east) coordinates. For example, if the lens were at $\pi_{\rm rel} = 2\,{\rm mas}$, this difference would be more than $10\,{\rm mas\,yr^{-1}}$.

High resolution imaging of the lens system would yield more definitive information. Immediate high resolution imaging could determine whether the blend is significantly offset from the source with much better constraints than we found in Section 8.1. If the blend is indeed separated by $\Delta\theta = 120\,{\rm mas}$, it would easily be resolved. If the high-resolution imaging is done in the optical (e.g., with the *Hubble Space Telescope*) and if the blend is separated from the source, then one could subtract the source flux (known from the microlensing solution) from the combined light at the position of the source, in order to measure the flux of the lens (or at least put much better limits on it). Since the lens is moving at $\mu_{\rm rel} = 18\,{\rm mas\,yr^{-1}}$, it could be resolved within 4 years (Batista et al. 2015; Bennett et al. 2015). Moreover, if the blend is now separated from the source, combined first plus second epoch of high-resolution imaging could determine whether the blend has the same proper motion as the host and so is a companion to it.

The final scenario is that the host is a white dwarf of, e.g., $M = 0.6\,M_\odot$, placing it at $D_L \sim 1.1\,{\rm kpc}$. Depending on its age and the instrument with which it is observed, it will likely be either very faint or invisible. However, in either case this would be an important discovery. And in the latter case, deeper observations could then be undertaken to discriminate between brown dwarf and white dwarf scenarios.

9. CONCLUSION

High-cadence $\Gamma = 6\,{\rm hr^{-1}}$ observations by KMTNet resolved the extremely short $2t_{\rm cc} = 33\,{\rm minute}$ caustic crossing of the planetary event OGLE-2015-BLG-0954. This proved crucial to both the measurement of the Einstein radius ($\theta_{\rm E} = 1.7\,{\rm mas}$) and to the arguments that the lens must be in the near disk (from the high proper motion $\mu_{\rm rel} = 18\,{\rm mas\,yr^{-1}}$). Hence, it was crucial both to the mass estimates of the host ($0.33 \pm 0.12\,M_\odot$) and planet ($3.9 \pm 1.4\,M_{\rm jup}$), and to the recognition that the lens and source will be separately resolvable in just a few years.

While such short caustic crossings are relatively rare, they are more likely to lead to complete mass and distance solutions than for typical events. This is because the most likely reason for the short crossing time is very high lens-source proper motion, which in turn is most likely due to a very nearby lens. It is easy to measure the flux of such nearby lenses if they are of relatively high mass. On the other hand if they are low mass, their microlens parallax (Gould 1992)

$$\pi_{\rm E} = \frac{\pi_{\rm rel}}{\theta_{\rm E}} = \sqrt{\frac{\pi_{\rm rel}}{\kappa M}} \qquad (16)$$

will be large and hence more easily measurable. Either of these effects can provide the second parameter needed for a complete solution, provided that the Einstein radius has been measured by resolving the caustic crossing.

In the case of OGLE-2015-BLG-0954, we were able to constrain the mass of the lens from the limit on lens light. No parallax effects were detected in the light curve. Hence, we could not obtain a definitive measurement. Instead we estimated the lens mass and distance based on kinematic arguments from its high proper motion. These are consistent with independent arguments derived from upper limits on lens light. They are also consistent with a white dwarf host, although this would be more surprising. The nature of the lens can be completely resolved in a few years based on high resolution imaging.

ACKNOWLEDGMENTS

This research has made use of the KMTNet system operated by KASI and the data were obtained at three host sites of CTIO in Chile, SAAO in South Africa, and SSO in Australia.

This work was supported by KASI (Korea Astronomy and Space Science Institute) grant 2016-1-832-01.

Work by J. C. Y. was performed under contract with the California Institute of Technology (Caltech)/Jet Propulsion Laboratory (JPL) funded by NASA through the Sagan Fellowship Program executed by the NASA Exoplanet Science Institute.

The OGLE team thanks Profs. M. Kubiak and G. Pietrzyński, former members of the OGLE team, for their contribution to the collection of the OGLE photometric data over the past years.

The OGLE project has received funding from the National Science Centre, Poland, grant MAESTRO 2014/14/A/ST9/00121 to A. U.

A. G. acknowledges support from NSF grant AST-1516842.

REFERENCES

Alard, C., & Lupton, R. H. 1998, A Method for Optimal Image Subtraction, ApJ, 503, 325

Albrow, M. D., Horne, K., Bramich, D. M., et al., 2009, Difference Imaging Photometry of Blended Gravitational Microlensing Events with a Numerical Kernel, MNRAS, 397, 2099

Batista, V., Beaulieu, J.-P., Bennett, D. P., et al. 2015, Confirmation of the OGLE-2005-BLG-169 Planet Signature and Its Characteristics with Lens-Source Proper Motion Detection, ApJ, 808, 170

Bennett, D. P., Bond, I. A., Udalski, A., et al., A Low-Mass Planet with a Possible Sub-Stellar-Mass Host in Microlensing Event MOA-2007-BLG-192, ApJ, 684, 663

Bennett, D. P., Rhie, S. H., Nikolaev, S., et al. 2010, Masses and Orbital Constraints for the OGLE-2006-BLG-109Lb,c Jupiter/Saturn Analog Planetary System, ApJ, 713, 837

Bennett, D. P., Bhattacharya, A., Anderson, J., et al. 2015, Confirmation of the Planetary Microlensing Signal and Star and Planet Mass Determinations for Event OGLE-2005-BLG-169, ApJ, 808, 169

Bensby, T., Yee, J. C., Feltzing, S., et al. 2013, Chemical Evolution of the Galactic Bulge as Traced by Microlensed Dwarf and Subgiant Stars. V. Evidence for a Wide Age Distribution and a Complex MDF, A&A, 549, A147

Bessell, M. S., & Brett, J. M. 1988, JHKLM Photometry - Standard Systems, Passbands, and Intrinsic Colors, PASP, 100, 1134

Bond, I. A., Udalski, A., Jaroszyński, M., et al. 2004, OGLE 2003-BLG-235/MOA 2003-BLG-53: A Planetary Microlensing Event, ApJ, 606, L155

Dominik, M. 1999, The Binary Gravitational Lens and Its Extreme Cases, A&A, 349, 108

Gaudi, B. S., Bennett, D. P., Udalski, A., et al. 2008, Discovery of a Jupiter/Saturn Analog with Gravitational Microlensing, Science, 319, 927

Gould, A. 1992, Extending the MACHO Search to about 10 exp 6 Solar Masses, ApJ, 392, 442

Gould, A., & Loeb, A. 1992, Discovering planetary systems through gravitational microlenses, ApJ, 396, 104

Gould, A., Udalski, A., Monard, B., et al. 2013, The Extreme Microlensing Event OGLE-2007-BLG-224: Terrestrial Parallax Observations of a Thick-Disk Brown Dwarf, ApJ, 698, L147

Gould, A., Dong, S., Gaudi, B. S., et al. 2010, Frequency of Solar-Like Systems and of Ice and Gas Giants Beyond the Snow Line from High-Magnification Microlensing Events in 2005-2008, ApJ, 720, 1073

Griest, K., & Safizadeh, N. 1998, The Use of High-Magnification Microlensing Events in Discovering Extrasolar Planets, ApJ, 500, 37

Henderson, C. B., Gaudi, B. S., Han, C., et al. 2014, Optimal Survey Strategies and Predicted Planet Yields for the Korean Microlensing Telescope Network, ApJ, 794, 52

Kervella, P., Thévenin, F., Di Folco, E., & Ségransan, D. 2004, The Angular Sizes of Dwarf Stars and Subgiants. Surface Brightness Relations Calibrated by Interferometry, A&A, 426, 297

Kim, S.-L., Lee, C.-U., Park, B.-G., et al. 2016, KMTNet: A Network of 1.6 m Wide-Field Optical Telescopes Installed at Three Southern Observatories, JKAS, 49, 37

Nataf, D. M., Gould, A., Fouqué, P., et al. 2013, Reddening and Extinction toward the Galactic Bulge from OGLE-III: The Inner Milky Way's RV $\sim$ 2.5 Extinction Curve, ApJ, 769, 88

Raghavan, D., McAlister, H. A., Henry, T. J., et al. 2010, A Survey of Stellar Families: Multiplicity of Solar-Type Stars, ApJS, 190, 1

Schechter, P. L., Mateo, M., & Saha, A. 1993, DOPHOT, a CCD Photometry Program: Description and Tests, PASP, 105, 1342

Shvartzvald, Y., & Maoz, D. 2012, Second-Generation Microlensing Planet Surveys: a Realistic Simulation, MNRAS, 419, 3631

Shvartzvald, Y., Udalski, A., Gould, A., et al. 2015, Spitzer Microlens Measurement of a Massive Remnant in a Well-Separated Binary, ApJ, 814, 111

Shvartzvald, Y., Maoz, D., Udalski, A., et al. 2016, The Frequency of Snowline-Region Planets from Four Years of OGLE-MOA-Wise Second-Generation Microlensing, MNRAS, 457, 4089

Skowron, J., Udalski, A., Szymański, M. K., et al. 2013, New Method to Measure Proper Motions of Microlensed Sources: Application to Candidate Free-floating-planet Event MOA-2011-BLG-262, ApJ, 785, 156

Szymański, M. K., Udalski, A., Soszyński, I., et al. 2011, The Optical Gravitational Lensing Experiment. OGLE-III Photometric Maps of the Galactic Bulge Fields, Acta Astron., 61, 83

Udalski, A. 2003, The Optical Gravitational Lensing Experiment. Real Time Data Analysis Systems in the OGLE-III Survey, Acta Astron., 53, 291

Udalski, A., Szymański, M., Kaluzny, J., et al. 1994, The Optical Gravitational Lensing Experiment. The Early Warning System: Real Time Microlensing, Acta Astron., 44, 227

Yee, J. C., Udalski, A., Sumi, T., et al. 2009, Extreme Magnification Microlensing Event OGLE-2008-BLG-279: Strong Limits on Planetary Companions to the Lens Star, ApJ, 703, 2082

Yee, J. C., Svartzvald, Y., Gal-Yam, A., et al. 2012, MOA-2011-BLG-293Lb: A Testbed for Pure Survey Microlensing Planet Detections, ApJ, 755, 102

Yoo, J., DePoy, D. L., Gal-Yam, A., et al. 2004, OGLE-2003-BLG-262: Finite-Source Effects from a Point-Mass Lens, ApJ, 603, 139

Zhu, W., Penny, M., Mao, S., Gould, A., & Gendron, R. 2014, Predictions for Microlensing Planetary Events from Core Accretion Theory, ApJ, 788, 73

Zhu, W., Calchi Novati, S., Gould, A., et al. 2016, Mass Measurements of Isolated Objects from Space-Based Microlensing, ApJ, in press, arXiv:1510.02097